

Evolution of the spin dynamics during freezing in the spin-glass $\text{Fe}_x\text{Cr}_{1-x}$

S. Säubert,^{1,2,*} C. Franz,^{1,2,3} J.K. Jochum,^{1,2} G. Benka,¹ A. Bauer,^{1,4} S.M. Shapiro,⁵ P. Böni,¹ and C. Pfleiderer^{1,4,6}

¹*Physik-Department, Technische Universität München, D-85748 Garching, Germany*

²*Heinz Maier-Leibnitz Zentrum, Technische Universität München, D-85748 Garching, Germany*

³*Jülich Centre for Neutron Science (JCNS) at Heinz Maier-Leibnitz Zentrum (MLZ),
Forschungszentrum Jülich GmbH, Garching, Germany*

⁴*Zentrum für QuantumEngineering (ZQE), Technische Universität München, D-85748 Garching, Germany*

⁵*Brookhaven National Laboratory, Department of Physics, Upton, NY 11973, USA*

⁶*Munich Center for Quantum Science and Technology (MCQST),
Technische Universität München, D-85748 Garching, Germany*

(Dated: January 12, 2023)

In the iron–chromium system, $\text{Fe}_x\text{Cr}_{1-x}$, a wide dome of spin-glass behavior emerges when the ferromagnetism of iron is suppressed and the antiferromagnetism of chromium emerges as a function of increasing iron content x . As both, the high-temperature state and the characteristic cluster size vary as a function of x , different regimes of spin-glass behavior may be compared in a single, isostructural material system. Here, we report a study of the spin dynamics across the freezing process into the spin-glass state for different iron concentrations ($x = 0.145, 0.175, 0.21$) using Modulation of Intensity with Zero Effort (MIEZE) spectroscopy. In the parameter range studied, the relaxation process observed experimentally may be described well in terms of a stretched exponential. In the reentrant cluster-glass regime, $x = 0.145$, this behavior persists up to high temperatures. In comparison, in the superparamagnetic regime, $x = 0.175$ and $x = 0.21$, a single relaxation time at elevated temperatures is observed. For all samples studied, the spin relaxation exhibits a momentum dependence consistent with a power law, providing evidence of a dispersive character of the spin relaxation.

A. Introduction

In spin-glasses, the combination of random site occupation and disorder with competing interactions, anisotropy, and frustration leads to a collective freezing of the spins in random orientations at the glass temperature T_g ^{1,2}. The freezing process may involve a broad distribution of relaxation times, resulting from varying correlation lengths of the individual magnetic clusters. These clusters may vary strongly in size, ranging from individual spins in canonical spin-glasses, over interacting clusters of spins in cluster glasses, to collectively behaving domains in superparamagnetic systems³. In dilute spin-glasses, the perhaps most comprehensively studied class of glassy magnetic systems^{4–12}, the relaxation times of the spin freezing exhibit no dispersion due to the short range of the interactions.

Seminal studies of the spin-glass behavior in $\text{Cu}_{1-x}\text{Mn}_x$ ($x = 0.1, 0.16, \text{ and } 0.35$) as well as $\text{Au}_{1-x}\text{Fe}_x$ ($x = 0.14$) using neutron spin echo (NSE) spectroscopy^{11,13} suggested non-exponential relaxation. To go beyond an account of the spin relaxation in terms of a stretched exponential, which cannot distinguish between a distribution of parallel relaxation channels and hierarchical relaxation comprising intercluster and intra-cluster processes, the Weron model¹⁴ was found to provide a universal description. This raises the question for key characteristics of the spin relaxation when the concentration of magnetic atoms is increased to form cluster-glass or superparamagnetic systems. Moreover, reports of a momentum independent quasielastic peak in the spin-glass regime^{15–20} contrast dispersive behavior

that has been attributed to either the coexistence of ferromagnetism and spin-glass behavior^{21–23} or momentum-dependent dynamics of the spin-glass²⁴.

To advance these questions, we report a study of the spin-glass dynamics in $\text{Fe}_x\text{Cr}_{1-x}$. When combining the itinerant-electron ferromagnet iron and the spin-density wave antiferromagnet chromium in the isostructural alloy $\text{Fe}_x\text{Cr}_{1-x}$, the ferromagnetic transition temperature is suppressed and long-range spin-density wave order emerges with increasing x for $x_c = 0.15 - 0.17$ ^{25–30}. A dome of spin-glass behavior is located at low temperatures in the vicinity of x_c ^{16,31–37}. The dome extends from $x \sim 0.10$ to $x \sim 0.25$, reaching well into concentration regimes which exhibit ferromagnetic and antiferromagnetic order at higher temperatures, respectively^{38–41}. Thus, for different x , the spin-glass behavior in $\text{Fe}_x\text{Cr}_{1-x}$ may emerge with decreasing temperature from ferromagnetic or antiferromagnetic order due to spin freezing^{42–45}. Moreover, the ferromagnetically ordered clusters initially grow in size as a function of increasing x , changing the character of the spin-glass state from a cluster-glass to a superparamagnet^{41,46,47}. As both iron and chromium display spin wave dispersions that are prototypical for ferro- and antiferromagnetism, respectively, a question concerns the existence and character of dispersive behavior in the spin-glass regime^{48–55}.

Quasielastic neutron scattering has been established as an indispensable tool in the study of spin relaxation processes. For a wide range of relaxation times expected in spin-glasses, neutron spin-echo spectroscopy appears to be ideally suited, since the associated measurements of the intermediate scattering function $S(q, \tau)$, as opposed to the dynamic structure factor $S(q, \hbar\omega)$, allows to sep-

arate dynamic processes on very different time scales. However, in conventional neutron spin-echo spectroscopy depolarizing samples or samples under depolarizing sample environment may only be measured at a high penalty in neutron flux^{56,57}. On this note, Modulation of Intensity with Zero Effort^{58,59} (MIEZE) is a spin-echo technique which permits measurements under depolarizing conditions for small momentum transfers. It is therefore ideally suited for the study of spin relaxation dynamics in nearly ferromagnetic and ferromagnetic systems.

In the study reported in this paper, we used the longitudinal MIEZE technique to determine the spin dynamics in $\text{Fe}_x\text{Cr}_{1-x}$ as a function of temperature for three different compositions. For the reentrant cluster-glass ($x = 0.145$), a broad distribution of relaxation times is observed over the entire temperature range that may be described well in terms of a stretched exponential. For compositions in the superparamagnetic regime ($x = 0.175$ and $x = 0.21$), a broad distribution of relaxation times at low temperatures that may be described well in terms of a stretched exponential is contrasted by a single relaxation time at elevated temperatures. Our data recorded in the sample with $x = 0.175$ are consistent with an earlier study using transverse NRSE and conventional NSE in the same sample¹², which, however exhibited more scatter and covered a smaller dynamical range. For all three compositions we find dispersive behavior of the spin relaxation that follows a power-law dependence of the momentum, q , consistent with $\Gamma \propto q^z$, where the dynamical exponent z decreases from $z \sim 1.5$ to $z \sim 1.0$ with increasing x . This behavior is loosely reminiscent of the quasielastic linewidth in $\text{Fe}_{0.7}\text{Al}_{0.3}$ ²⁴. However, for $\text{Fe}_x\text{Cr}_{1-x}$ the origin of the dispersive behavior may, in principle, comprise a combination of different contributions.

Our paper is organized as follows. In Section B, specific aspects of the neutron scattering experiments and the crystal growth techniques are presented. In Sections C1 and C2 the elastic and quasielastic neutron scattering experiments are described. In Section D, the implications of the experiments are discussed, followed by a summary of the findings of this study in Section E.

B. Experimental Methods

Our experiments were conducted at the beamline RESEDA^{60,61} at the Heinz Maier-Leibnitz Zentrum using the longitudinal MIEZE option⁶². The MIEZE method is particularly well suited to study dynamics close to the $[0, 0, 0]$ Bragg peak, corresponding to small-angle neutron scattering (SANS)^{61,62}. In Fig.1 the experimental setup used for our experiments is shown. The sample-detector distance, $L_{\text{SD}} = 2.335$ m, was maximized to ensure highest q resolution. To provide high neutron flux and to cover the desired dynamic range, the wavelength was set to 6 \AA with a wavelength spread $\Delta\lambda/\lambda = 0.12$. In this configuration, a dynamic range

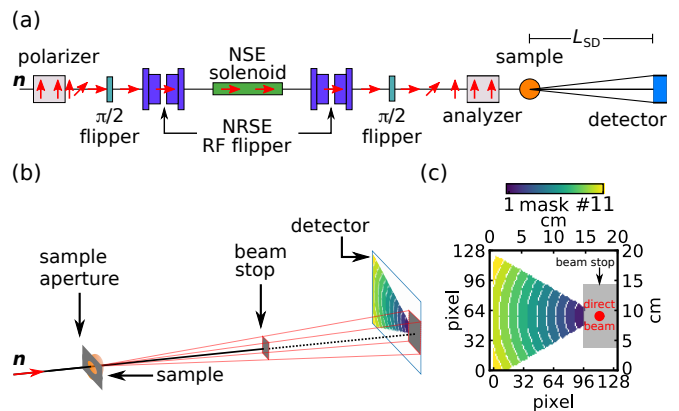


FIG. 1. Longitudinal MIEZE setup used in our experiments^{51,62}. (a) Schematic depiction of the spectrometer. All spin manipulations are performed upstream to the sample, rendering the method insensitive to depolarizing conditions at the sample position. The red arrows indicate the direction of the magnetic guide fields. (b) Schematic depiction of the neutron flight path through the spectrometer showing the sample aperture, sample, beam stop, and detector. (c) Detector segments used in the evaluation of the MIEZE scans. Segments represent parts of circular rings centered at the direct beam with an opening angle of 60° and a width of 10 pixels. The grey shaded area represents the location of the beam stop.

from $\sim 6 \cdot 10^{-6}$ ns to 2 ns was accessible. Fig. 1(b) shows a schematic of the neutron flight path through the spectrometer. Data were recorded with a $20 \text{ cm} \times 20 \text{ cm}$ 2D CASCADE detector⁶³, covering a q range from 0.016 \AA^{-1} to 0.085 \AA^{-1} at $\lambda = 6 \text{ \AA}$ and $L_{\text{SD}} = 2.335$ m. Recent developments at RESEDA made it possible to increase L_{SD} up to 3.43 m improving the spatial resolution further⁶¹.

The grouping of the detector segments for evaluating the quasielastic data are shown in Fig. 1(c). For the elastic measurements, the identical setup was used with narrower grouped detector segments, i.e., data were evaluated in the same area as in Fig. 1(c) but divided in 25 instead of 11 detector segments. The sample was cooled to temperatures between 4 K and 300 K using a top-loading closed-cycle refrigerator and the temperature was controlled with two sensors close to the sample. The temperature stability was ~ 0.05 K. No hysteresis was observed in temperature scans. Data were normalized using data recorded at the base temperature of ~ 4 K, assuming that the spin dynamics in $\text{Fe}_x\text{Cr}_{1-x}$ are frozen at temperatures well below T_g ¹¹. This procedure minimizes systematic errors since the experimental setup remains unchanged throughout the entire experiment on a given sample.

We investigated three textured polycrystalline samples of $\text{Fe}_x\text{Cr}_{1-x}$ containing large grains with iron concentrations of $x = 0.145$, 0.175 , and 0.21 . The samples were prepared by means of arc melting from pure starting materials and annealed for 4 days at 1100°C before quenching in water¹⁶. To remove strain, the samples were sub-

sequently annealed at 1000 °C for 1 day¹⁶. Following this process ingots of cylindrical shape with a height of approximately 20 mm and a diameter of about 10 mm were obtained.

To optimize the signal-to-noise ratio, slabs with a thickness of 8 mm were cut from the ingots. A circular aperture made of cadmium with a diameter of 10 mm was attached directly to the samples. Thus, the neutron beam effectively illuminated samples of cylindrical shape with a diameter of 10 mm and a length of 8 mm, where the cylindrical axis was parallel to the incident neutron beam. Measurements on a sample with $x = 0.17$ from Benka *et al.*⁴¹ (not shown) were in excellent agreement with the results presented in the following.

Parts of the sample with $x = 0.145$ were recently used to investigate the influence of concentration fluctuations on relaxation processes in spin-glasses¹². Using atom probe tomography, a high-resolution local probe, together with neutron resonant spin-echo spectroscopy it was shown that small-scale inhomogeneities in the microstructure influence the relaxation processes of a spin-glass material¹². Using the Weron model which had previously been applied to dilute spin-glasses¹³, the relaxation processes were described in this study.

C. Experimental Results

The phase diagram of $\text{Fe}_x\text{Cr}_{1-x}$ as a function of temperature and iron concentration x is shown in Fig. 2(a) as reproduced from literature^{36,38-41}. For comparison, the temperature dependence of the integrated SANS intensity of the three samples measured in this study is shown in Figs. 2(b) to 2(d). At the border between ferromagnetic and antiferromagnetic order, a dome of spin-glass behavior emerges, covering the regime of putative quantum phase transitions. At low temperatures, this spin-glass regime includes concentrations for which at high temperatures long-range ferromagnetic or antiferromagnetic order are observed.

In our study, three compositions were investigated: (i) $x = 0.145$ which exhibits transitions from paramagnetism (PM) to antiferromagnetism (AFM) to a spin-glass (SG) with a glass temperature $T_g = 11 \text{ K} \pm 2 \text{ K}$ ⁴¹, (ii) $x = 0.175$ which exhibits transitions from PM via a small region reminiscent of FM order⁴¹ to a SG with a glass temperature $T_g = 20 \text{ K} \pm 2 \text{ K}$ ⁴¹, and (iii) $x = 0.21$ which exhibits transitions from PM to ferromagnetism (FM) to a SG with a glass temperature $T_g = 14 \text{ K} \pm 2 \text{ K}$ ⁴¹.

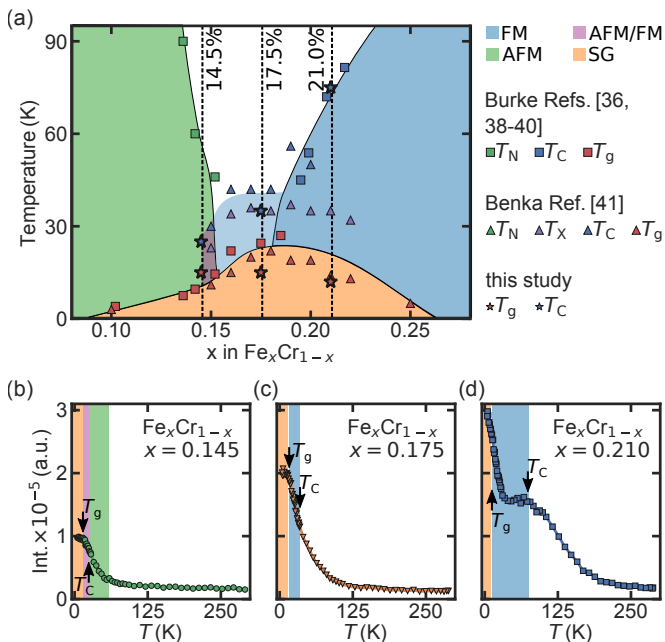


FIG. 2. Magnetic properties of the $\text{Fe}_x\text{Cr}_{1-x}$ system. Antiferromagnetic (AFM, green), ferromagnetic (FM, blue), spin-glass (SG, orange), and antiferromagnetic-ferromagnetic (AFM/FM, purple) regimes are distinguished. (a) Temperature vs concentration phase diagram combining data from neutron scattering and low-field magnetization by Burke *et al.* (squares)^{36,38-40}, ac susceptibility and magnetization by Benka *et al.* (triangles)⁴¹, and neutron scattering (present work, stars). (b)-(d) Integrated SANS intensity for the three samples measured at RESEDA. The shaded areas indicate magnetic regimes as inferred from the phase diagram.

1. Elastic Scattering

The temperature dependence of the integrated SANS intensity is shown in Figs. 2(b) to 2(d). As no magnetic scattering was observed at high temperatures, the data recorded at $\sim 300 \text{ K}$ were used for background subtraction.

The scattered intensities as a function of temperature for $x = 0.145$ and $x = 0.175$ behave similarly. With decreasing temperature the intensity increases as expected for a transition into a ferromagnetically ordered state. When entering the spin-glass state, the system becomes static on the time scales probed by SANS, and the intensity increases with a change in slope, forming a plateau that starts at the onset of the spin-glass regime⁶⁴.

The bulk properties and phase diagram show that the sample with $x = 0.145$ enters the spin-glass regime via an antiferromagnetic state, which may not be identified microscopically for the parameter range probed in SANS. Interestingly, the increase in intensity is, analogous to the sample with $x = 0.175$, reminiscent of ferromagnetic order in agreement with Ref. [41].

For the sample with $x = 0.21$, a broad feature with a maximum at $\sim 75 \text{ K}$ defines T_C , followed by a sharp increase in intensity. A change of slope with decreasing temperature, close to the transition temperature reported previously in Ref. [41], defines T_g . The signatures defined in neutron scattering are denoted by stars in Fig. 2(a). Discrepancies as compared to the phase boundaries inferred from the ac susceptibility and magnetization⁴¹ may reflect the different time scales probed by the different methods.

The q dependence of the SANS data, cf. Section B for details on data analysis, is shown in Figs. 3(a) to 3(c) for different temperatures. Following the approach taken in related SANS studies on other materials^{65,66} we consider a single power law form

$$I \propto q^{-n}. \quad (1)$$

Fitting the experimental data yields exponents as a function of temperature as shown in Figs. 3(d) to 3(f).

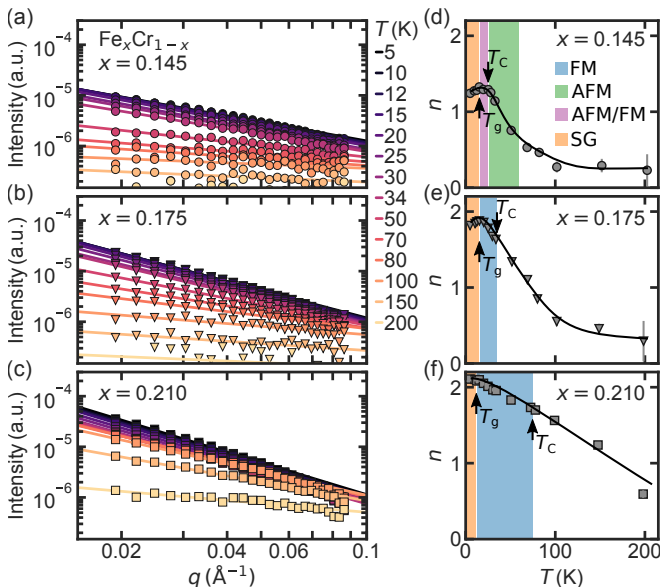


FIG. 3. Momentum dependence of SANS of $\text{Fe}_x\text{Cr}_{1-x}$ as measured at RESEDA. (a)-(c) Intensity as a function of scattering vector q . The accessible q range was $0.02 \text{ \AA}^{-1} < q < 0.08 \text{ \AA}^{-1}$. Solid lines are fits using Eq. (1). (d)-(f) Temperature dependence of the exponent n obtained from the fits in (a)-(c). Solid lines are guides to the eye. The shaded areas indicate the regimes according to the phase diagram, namely AFM (green), AFM/FM (purple), FM (blue), and SG (orange). Samples with iron concentrations of $x = 0.145$ (top row), $x = 0.175$ (middle row), and $x = 0.21$ (bottom row) were evaluated at different temperatures.

With decreasing temperature, the exponent n increases from ~ 0.3 , reaching low-temperature values of $n \sim 1.3$ for $x = 0.145$, $n \sim 1.8$ for $x = 0.175$, and $n \sim 2.1$ for $x = 0.21$. Even though the data are well-described by the power law in Eq. (1), unambiguous interpretation of the exponent n proves difficult. Assuming a two-phase system where smooth clusters are isolated, $n = 4$ would be expected. Deviations from this behavior would indicate more complex phases including fractal surfaces. An exponent of $n = 2$, for instance, was reported in the perovskite manganite $\text{Pr}_{1-x}\text{Ca}_x\text{MnO}_3$ and attributed to sheets of inter-penetrating ferromagnetic and antiferromagnetic phases⁶⁵. In the same material, Viret *et al.*⁶⁶ found $n = 1.6 - 1.7$ which was attributed to filamentary ferromagnetic chains in analogy to polymers. An increase

in n with decreasing temperature suggests a coarsening of the interfaces as the system enters the spin-glass regime, consistent with an increase in cluster size.

To address the question of the nature of the low-temperature magnetic structure as a function of iron concentration, it may be necessary to collect data at even smaller q values, which is beyond the technical limits of the work reported here. Alternatively, more complex dependencies, e.g., comprising several different power-law contributions may be possible. Such descriptions would require theoretical modelling beyond the scope of our study.

2. Quasielastic Measurements

The normalized intermediate scattering function,

$$I(q, \tau) = S(q, \tau)/S(q, 0), \quad (2)$$

in the temperature range $4 \text{ K} \leq T \leq 150 \text{ K}$ for $q = 0.044 \text{ \AA}^{-1}$ and all $\text{Fe}_x\text{Cr}_{1-x}$ compositions investigated is shown in Fig. 4. Following careful comparison of the data with different relaxation models^{4,6-8,10,11,13,67} we find that the data are already described well by a stretched exponential characteristic of a distribution of relaxation rates, namely

$$I(q, \tau) = I_{\text{elastic}} + (1 - I_{\text{elastic}}) \exp\left(-(\Gamma\tau)^\beta\right). \quad (3)$$

Here, Γ is the decay rate, corresponding to the inverse spin relaxation time, $0 < \beta \leq 1$ stretches the classic exponential decay ($\beta = 1$), and the prefactor I_{elastic} describes the elastic contribution to the signal. In the light of the microscopic complexity of the $\text{Fe}_x\text{Cr}_{1-x}$ system, which may support both parallel as well as hierarchical relaxation, we refrain from an analysis in terms of more sophisticated mechanisms as assumed in the Weron model^{12-14,67}.

The normalized intermediate scattering functions in Fig. 4 have been shifted vertically in steps of 0.25 for better visibility. Fig. 4(a) shows the sample with $x = 0.145$. The intermediate scattering function is constant below $\sim 4 \text{ K}$, confirming that the spin dynamics are frozen¹¹ with respect to the normalizing data at 4 K. For temperatures around the glass temperature, $T_g \sim 15 \text{ K}$, the sample starts to show signatures of dynamic behavior, notably spin relaxation as indicated by a decrease in the intermediate scattering function. The relaxation time of the spins is inferred from a fit to the data using $\tau = \frac{\hbar}{\Gamma}$. Increasing the temperature shifts the spin relaxation to shorter spin-echo times. I_{elastic} describes the elastic contribution to the intermediate scattering function, corresponding to the fraction of the sample that is static on the time scales probed here, i.e., clusters fluctuating on much longer time scales.

The elastic signal decreases with increasing temperature, reaching a minimum of $I_{\text{elastic}} \approx 0.25$ for temperatures above 34 K. For all temperatures, the system may

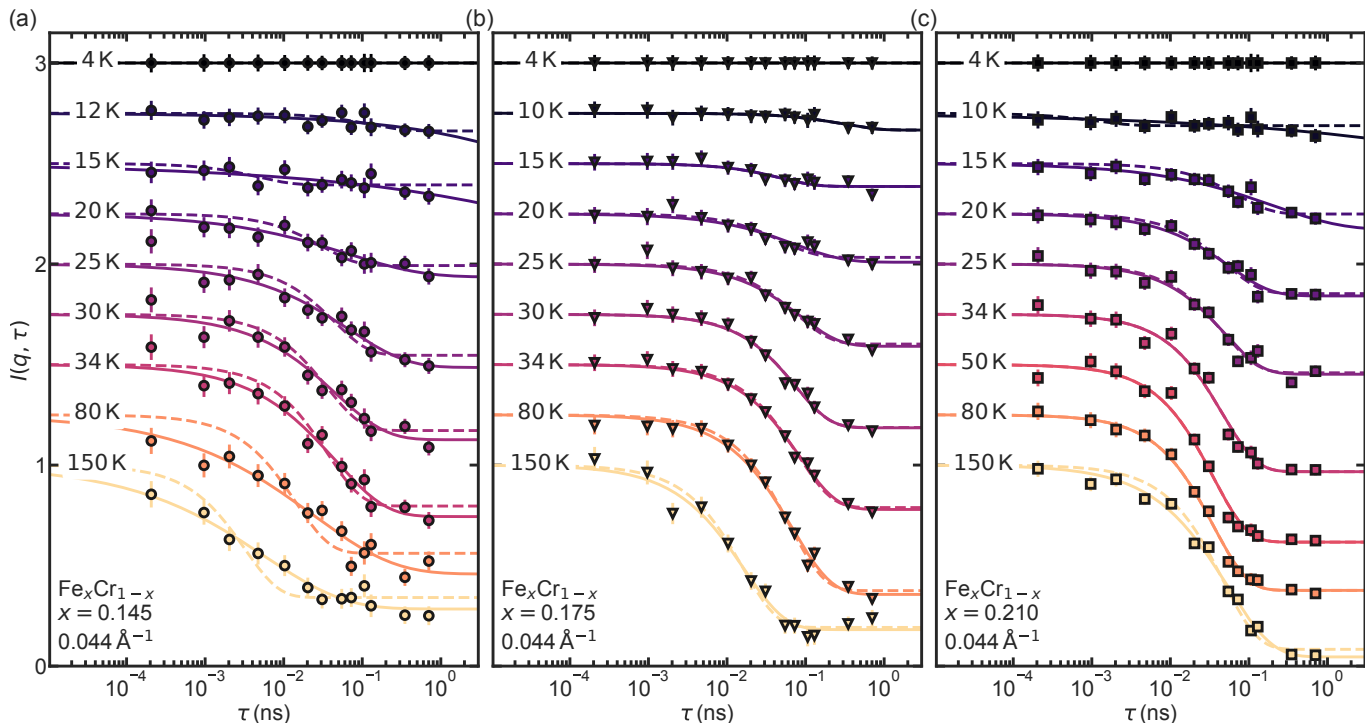


FIG. 4. Normalized intermediate scattering function as measured for different temperatures in $\text{Fe}_x\text{Cr}_{1-x}$. Data were recorded using neutrons with a mean wavelength of $\lambda = 6.0 \text{ \AA}$ and are shown at $q = 0.044 \text{ \AA}^{-1}$ for (a) $x = 0.145$, (b) $x = 0.175$, (c) $x = 0.21$. For better visibility, data are shifted vertically. The solid lines are fits to the data using the stretched exponential in Eq. (3). The dashed lines represent fits using a single exponential relaxation, corresponding to $\beta = 1$ in Eq. (3).

be described by a stretched exponential decay, $\beta < 1$. To highlight the need for the stretching parameter β , exponential decays ($\beta = 1$) are shown for comparison as dashed lines in Figs. 4(a) to 4(c). The deviation from simple exponential behavior gets more pronounced with decreasing temperature.

The intermediate scattering functions for the sample with $x = 0.175$ are shown in Fig. 4(b). For temperatures below T_g , the data resemble the behavior observed for $x = 0.145$. Under increasing temperature the spin relaxation is similarly shifted to shorter times but remains larger than for $x = 0.145$. The minimum of the elastic background is reduced to $I_{\text{elastic}} \approx 0.15$. In contrast to the sample with $x = 0.145$, at higher temperatures the spin relaxation can be described by a simple exponential decay.

For $x = 0.21$, shown in Fig. 4(c), the behavior again is highly reminiscent of the other two compositions. Accordingly, we observe a shift of the relaxation time towards shorter times as the temperature increases. However, for temperatures above 50 K the relaxation time no longer decreases. The elastic contribution reaches a minimum of $I_{\text{elastic}} \approx 0.1$. In a paramagnetic sample, where all scattering is dynamic, the spin-echo curve would decay to $I_{\text{elastic}} = 0$ at high temperatures or long spin-echo times. The observed sample dependence of I_{elastic} may be attributed empirically to the different iron contents of the samples, which lead to different high-temperature

magnetic phases.

Since the measurements were performed in a SANS geometry, close to the ferromagnetic Bragg peak at $q = 0$, ferromagnetic fluctuations will contribute strongly to the measured intensity. However, as possible antiferromagnetic scattering intensity cannot be observed in the vicinity of $q = 0$, antiferromagnetic fluctuations will not contribute to the exponential decay, decreasing the dynamic contribution to the intensity in samples with a larger antiferromagnetic fraction. This observation is in accordance with the elastic measurements shown in Figs. 2(b) to 2(d), which indicate that the intensity increases with increasing iron content.

The temperature dependences of the fit parameters I_{elastic} and β are summarized in Fig. 5 for $q = 0.044 \text{ \AA}^{-1}$. For all samples the elastic contribution I_{elastic} decreases linearly with increasing temperature reaching a constant value above $\sim 40 \text{ K}$, i.e., far above the glass temperature. A shrinking elastic contribution with increasing temperature suggests that parts of the sample slowly unfreeze on the time scales studied in our experiments.

The exponent β provides an estimate of the broadening of the spectrum of relaxation times. For all samples, β decreases drastically when the temperature decreases towards the spin-glass regime. This evolution suggests an increase of the distribution of relaxation times, as expected of the formation of different-sized domains fluctuating on different time scales before freezing at the lowest

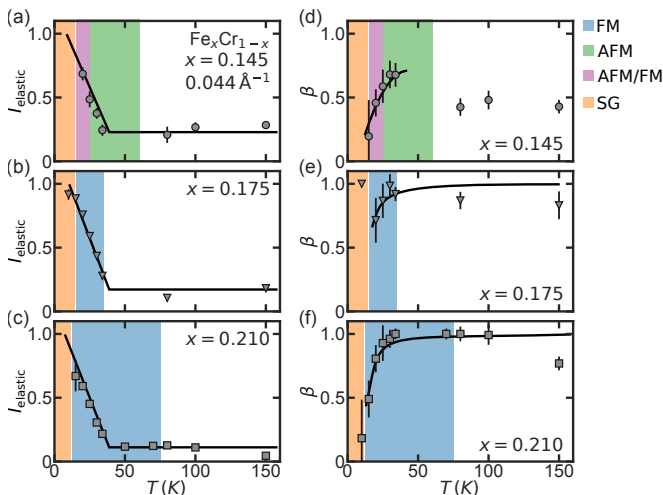


FIG. 5. Temperature dependence of the fit parameters I_{elastic} and β in Eq. (3) for the three $\text{Fe}_x\text{Cr}_{1-x}$ samples with (a),(d) $x = 0.145$, (b),(e) $x = 0.175$, and (c),(f) $x = 0.21$. Data are shown for $q = 0.044 \text{ \AA}^{-1}$. The shaded areas indicate the phases according to the phase diagram: AFM (green), AFM/FM (purple), FM (blue), and SG (orange). (a)-(c) Elastic contribution I_{elastic} as a function of temperature, showing a linear increase for temperatures below ~ 40 K. Solid lines are guides to the eye. The elastic background, i.e., the constant value at temperatures above 40 K, is connected to the magnetic signal-to-noise ratio, and thus different for the different samples, see main text for details. (d)-(f) Stretched exponent β as function of temperature showing a drastic decrease of β close to T_g . Solid lines are guides to the eye.

temperatures. For $x = 0.145$, β stays below 1 over the entire temperature range, while for the other two compositions β is close to 1 at temperatures above T_g . This means that the dynamics may be described with a single relaxation time.

Numerical calculations of the non-exponential relaxation in spin-glasses and glassy systems^{68,69} have shown that $\beta = 1/3$ is approached at T_g when the system is close to its percolation limit. The decrease of β we observe as the spin-glass regime is approached is in qualitative agreement with these calculations.

D. Discussion

The area detector used in our MIEZE measurements allowed studying the normalized intermediate scattering function $I(q, \tau)$ simultaneously over a wide range of momentum transfers q . The q dependence of the decay rate Γ and therefore the spin relaxation time is shown in Figs. 6(a) to 6(c). Within experimental accuracy, our data it are consistent with

$$\Gamma = Aq^z, \quad (4)$$

where q is the momentum transfer, z the dynamical exponent, and A the energy scale of the exchange interactions.

The decay rate Γ as a function of q , shown in Fig. 6, was fitted using Eq. (4) with fixed values of z , i.e., $z = 1.0$, $z = 1.5$, and $z = 2.0$, as well as with z as an independent fitting parameter. Additionally, data were fitted for each sample and for all temperatures independently, as well as simultaneously for all temperatures. The fit results are summarized in Tab. I. A χ^2 -analysis of the fits with fixed parameter z shows that with decreasing iron content z decreases from ~ 1.5 to ~ 1.0 , which is supported by the fits with z as a free parameter. The resulting values of z and A as a function of temperature are depicted in Figs. 6(d) to 6(i).

For small β , the distribution of relaxation times is very broad and the data cannot be described with a single τ . Therefore a meaningful linewidth Γ cannot be extracted for any of the three samples below and around the glass temperature T_g . For $x = 0.145$, Γ could only be extracted for a small temperature window in the ferromagnetic regime, $25 \text{ K} \leq T \leq 34 \text{ K}$. Even at these temperatures, the exponential decay is already stretched and the values of Γ determined experimentally represent a mean relaxation time rather than a single relaxation time. At higher temperatures, the exponential decay is strongly stretched such that a single dominant relaxation time could not be determined. The sample with $x = 0.175$ allowed us to analyze Γ for temperatures between $25 \text{ K} \leq T \leq 80 \text{ K}$. For $x = 0.21$, Γ could be extracted for all temperatures above the freezing temperature T_g .

For all concentrations, Γ depends on q according to the relation given in Eq. (4). The exponent z increases for increasing iron concentration from $z \approx 1$ to $z \approx 2$. According to dynamic scaling theory the critical exponent at T_c for pure ferromagnets in the limit $q \rightarrow 0$ corresponds to $z = 2.5$ while antiferromagnetic correlations for $q \rightarrow Q_{\text{AFM}}$ lead to $z = 1.5$. Heuristically, one might hence explain the exponents in $\text{Fe}_x\text{Cr}_{1-x}$ in terms of a competition of ferromagnetic and antiferromagnetic correlations.

Tajima *et al.* used a spin diffusion model with $\Gamma \propto q^{2.0}$ to describe the q dependence of Γ in the Invar alloy $\text{Fe}_{65}\text{Ni}_{35}$ over a rather wide q range⁷⁰. This model assumes a hydrodynamic behavior of uncorrelated spins. The authors argued that the system never reaches criticality, i.e., $z = 2.5$ for ferromagnetically correlated spins, due to impurity scattering of the electrons.

Along this line, the presence of chromium atoms acting as impurities in ferromagnetic iron clusters could prevent the system from reaching ferromagnetic critical dynamics, reducing z to 2.0. A large fraction of chromium, and therefore an increase in antiferromagnetic correlations in $\text{Fe}_x\text{Cr}_{1-x}$ could reduce the exponent z further towards 1.5 leading to an effective range of exponents between $z = 1.5$ for antiferromagnetic correlations and $z = 2.0$ as expected in the spin diffusion model. Values of z below 1 may reflect the large number of different time scales in spin-glasses. Unusually small values of z found in spin-glasses were previously attributed to disorder, the prox-

TABLE I. Summary of the fitting procedure of the spin dynamics in $\text{Fe}_x\text{Cr}_{1-x}$ using Eq. (4) with different approaches, namely: (i) fixing the exponent $z = 1.0$, (ii) fixing the exponent $z = 1.5$, (iii) fixing the exponent $z = 2.0$, (iv) leaving the exponent z as a free fit parameter. Additionally, data were also fitted with (I) all temperatures independently and (II) all temperatures simultaneously. The χ^2 value of each fit is used as an indicator for the goodness of the fits.

$\text{Fe}_x\text{Cr}_{1-x}$ with $x = 0.145$; all temperatures fitted independently

T (K)	$z = 1.0$					$z = 1.5$					$z = 2.0$					$z = \text{free}$				
	A	A_{err}	z	z_{err}	χ^2	A	A_{err}	z	z_{err}	χ^2	A	A_{err}	z	z_{err}	χ^2	A	A_{err}	z	z_{err}	χ^2
25	273	10	1.0	—	1.20	1127	84	1.5	—	4.95	4394	506	2.0	—	11.19	223	61	0.9	0.1	1.13
30	333	48	1.0	—	18.63	1536	225	1.5	—	18.84	6576	1042	2.0	—	21.47	629	745	1.2	0.4	18.22
34	400	40	1.0	—	20.21	1723	184	1.5	—	22.79	6953	914	2.0	—	32.99	589	507	1.1	0.3	19.74

$\text{Fe}_x\text{Cr}_{1-x}$ with $x = 0.145$; all temperatures fitted simultaneously

T (K)	$z = 1.0$					$z = 1.5$					$z = 2.0$					$z = \text{free}$				
	A	A_{err}	z	z_{err}	χ^2	A	A_{err}	z	z_{err}	χ^2	A	A_{err}	z	z_{err}	χ^2	A	A_{err}	z	z_{err}	χ^2
all	336	22	1.0	—	51.27	1443	104	1.5	—	60.63	5794	498	2.0	—	82.4	377.0	190.0	1.0	0.2	51.18

$\text{Fe}_x\text{Cr}_{1-x}$ with $x = 0.175$; all temperatures fitted independently

T (K)	$z = 1.0$					$z = 1.5$					$z = 2.0$					$z = \text{free}$				
	A	A_{err}	z	z_{err}	χ^2	A	A_{err}	z	z_{err}	χ^2	A	A_{err}	z	z_{err}	χ^2	A	A_{err}	z	z_{err}	χ^2
25	233	17	1.0	—	7.60	1073	88	1.5	—	9.88	4663	537	2.0	—	18.63	293	249	1.1	0.3	7.54
30	212	12	1.0	—	12.51	950	29	1.5	—	3.94	3912	306	2.0	—	24.21	656	158	1.4	0.1	2.94
34	196	7	1.0	—	5.55	891	31	1.5	—	5.03	3877	273	2.0	—	20.56	445	178	1.3	0.1	3.34
80	239	13	1.0	—	15.82	1060	22	1.5	—	2.30	4484	213	2.0	—	12.26	1145	298	1.5	0.1	2.26

$\text{Fe}_x\text{Cr}_{1-x}$ with $x = 0.175$; all temperatures fitted simultaneously

T (K)	$z = 1.0$					$z = 1.5$					$z = 2.0$					$z = \text{free}$				
	A	A_{err}	z	z_{err}	χ^2	A	A_{err}	z	z_{err}	χ^2	A	A_{err}	z	z_{err}	χ^2	A	A_{err}	z	z_{err}	χ^2
all	216	6	1.0	—	55.92	973	22	1.5	—	33.46	4138	149	2.0	—	86.81	700	163	1.4	0.1	31.52

$\text{Fe}_x\text{Cr}_{1-x}$ with $x = 0.21$; all temperatures fitted independently

T (K)	$z = 1.0$					$z = 1.5$					$z = 2.0$					$z = \text{free}$				
	A	A_{err}	z	z_{err}	χ^2	A	A_{err}	z	z_{err}	χ^2	A	A_{err}	z	z_{err}	χ^2	A	A_{err}	z	z_{err}	χ^2
15	303	37	1.0	—	9.90	1495	173	1.5	—	9.14	6761	928	2.0	—	12.33	849	889	1.3	0.3	8.84
20	266	7	1.0	—	2.05	1204	61	1.5	—	6.80	5096	479	2.0	—	22.29	360	83	1.1	0.1	1.68
25	310	26	1.0	—	23.64	1504	83	1.5	—	10.65	6646	519	2.0	—	20.54	1462	742	1.5	0.2	10.64
30	311	15	1.0	—	11.96	1469	45	1.5	—	4.97	6321	511	2.0	—	33.39	844	149	1.3	0.1	2.26
34	338	24	1.0	—	29.58	1641	52	1.5	—	6.28	7232	457	2.0	—	24.47	1578	448	1.5	0.1	6.27
50	430	33	1.0	—	43.43	2011	66	1.5	—	8.49	8643	446	2.0	—	20.47	2393	764	1.6	0.1	8.20
70	418	37	1.0	—	43.72	2041	64	1.5	—	5.76	9099	392	2.0	—	10.77	3350	838	1.7	0.1	3.76
80	423	32	1.0	—	66.27	1952	48	1.5	—	7.52	8283	387	2.0	—	26.58	2506	565	1.6	0.1	6.48
100	383	25	1.0	—	54.38	1763	18	1.5	—	1.30	7499	327	2.0	—	24.07	1984	181	1.5	0.1	1.07
150	291	37	1.0	—	137.06	1457	78	1.5	—	27.54	6468	214	2.0	—	10.63	4169	1032	1.8	0.1	7.52

$\text{Fe}_x\text{Cr}_{1-x}$ with $x = 0.21$; all temperatures fitted simultaneously

T (K)	$z = 1.0$					$z = 1.5$					$z = 2.0$					$z = \text{free}$				
	A	A_{err}	z	z_{err}	χ^2	A	A_{err}	z	z_{err}	χ^2	A	A_{err}	z	z_{err}	χ^2	A	A_{err}	z	z_{err}	χ^2
all	348	10	1.0	—	610.23	1659	31	1.5	—	256.94	7203	163	2.0	—	363.71	2205	364	1.6	0.1	249.2

imity to the spin-glass transition or a reentrant phase, or the complex character of the interactions^{71,72}.

A q dependence of Γ has, finally, been reported by Bao *et al.*, who found that the spin dynamics in $\text{Fe}_{0.7}\text{Al}_{0.3}$ can be approximated with $\Gamma \propto q^{2.5}$ for q values from $0.05 \text{ \AA}^{-1} - 0.5 \text{ \AA}^{-1}$. This finding is in contrast to studies of dilute spin-glasses which reported that the relaxation process does not depend on q . Such a result is expected

for dilute systems that are homogeneous over the q scale studied.

E. Conclusions

In summary, we reported a MIEZE spectroscopy study of the spin dynamics in $\text{Fe}_x\text{Cr}_{1-x}$ samples with $x =$

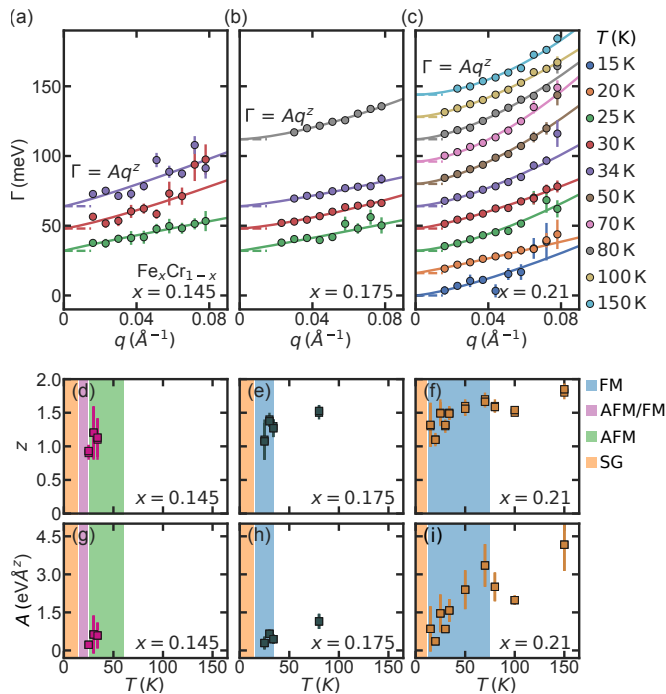


FIG. 6. Momentum dependence of the decay rate Γ . Data are shown for (a) $x = 0.145$, (b) $x = 0.175$, and (c) $x = 0.21$ and temperatures where a meaningful linewidth Γ could be extracted, see main text for details. The solid lines are fits to the data using Eq. (4). The temperature dependence of the fit parameters z and A are shown for $x = 0.145$ (left column), $x = 0.175$ (middle column), and $x = 0.21$ (right column). The shaded areas indicate the phases according to the phase diagram: AFM (green), AFM/FM (purple), FM (blue), and SG (orange).

0.145, $x = 0.175$, and $x = 0.21$. These compositions were chosen to compare the spin relaxation for different spin-glass classifications and reentrant temperature dependencies from different high-temperature properties, namely antiferromagnetic, paramagnetic, and ferromagnetic states. The dynamic properties of all samples studied are consistent with a comprehensive study of polycrystalline samples⁴¹. Properties of the sample with $x = 0.175$ have been reported in Ref. [12] using transverse NRSE and conventional NSE featuring more scatter and a smaller dynamic range. All samples show a broad distribution of relaxation times close to the spin-glass regime which, in the simplest approach, can be described by a stretched exponential. The stretching exponent β

approaches $1/3$ as the spin-glass regime is approached, suggesting proximity to the percolation limit. For increasing iron content and hence increasing tendency to ferromagnetic order, the spin relaxation can be described with a simple exponential (Debye) decay at high temperatures, where a single relaxation time can be extracted, indicating a smaller spread in relaxation times and magnetic cluster sizes. As explained above we refrain from an analysis in terms of more specific mechanisms as assumed, e.g., in the Weron model.

The spin relaxation dynamics of all three compositions x investigated in our study depends on q . Such a dependence contrasts dilute spin-glasses in which no dispersive behavior has been observed⁹. Within the scatter of our data the dispersive behavior may be described by a power-law dependence where the exponent z decreases with increasing iron concentration. We note, however, that the dispersive character may be the result of a combination of different contributions with different values of z , a scenario that we cannot disentangle further.

On a technical note, the present study highlights that the MIEZE technique allows to perform high-resolution neutron spin-echo spectroscopy over a large dynamic range in materials hosting ferromagnetic domains that may depolarize the neutron beam, posing a major limitation in conventional neutron spin-echo spectroscopy. Samples with ferromagnetic, antiferromagnetic, or paramagnetic high-temperature properties may therefore be investigated using MIEZE with the same instrument and sample environment.

ACKNOWLEDGMENTS

We wish to thank F. Haslbeck, M. Mantwill, S. Mayr, S. Mühlbauer, and A. Wendl for fruitful discussions and assistance with the experiments. This work has been funded by the Deutsche Forschungsgemeinschaft (DFG, German Research Foundation) under TRR80 (From Electronic Correlations to Functionality, Project No. 107745057, Project E1) and the excellence cluster MCQST under Germany's Excellence Strategy EXC-2111 (Project No. 390814868). Financial support by the Bundesministerium für Bildung und Forschung (BMBF) through Project No. 05K16WO6 as well as by the European Research Council (ERC) through Advanced Grants No. 291079 (TOPFIT) and No. 788031 (ExQuiSid) is gratefully acknowledged. G.B. and S.S. acknowledge financial support through the TUM Graduate School.

* steffen.saeubert@gmail.com

¹ P. Nordblad, Competing Interaction in Magnets: The Root of Ordered Disorder or only Frustration? *Physica Scripta* **88**, 058301 (2013).

² J. A. Mydosh, Spin Glasses: Redux: An Updated Experimental/Materials Survey, *Rep. Prog. Phys.* **78**, 052501

(2015).

³ J. S. McCloy, Spin and Ferroic Glasses, in *Springer Handbook of Glass*, edited by J. D. Musgraves, J. Hu, and L. Calvez (Springer International Publishing, Cham, 2019) pp. 687–718.

⁴ F. Mezei and A. P. Murani, Combined Three-Dimensional

- Polarization Analysis and Spin Echo Study of Spin Glass Dynamics, *J. Magn. Magn. Mater.* **14**, 211 (1979).
- ⁵ A. P. Murani, F. Mezei, and J. L. Tholence, Neutron Spin Echo, Polarisation Analysis and A.C. Susceptibility Measurements of Spin Glass Dynamics, *Physica B+C* **108**, 1283 (1981).
 - ⁶ A. P. Murani, Spectral Distribution of Relaxation Times in Spin Glasses, *J. Magn. Magn. Mater.* **22**, 271 (1981).
 - ⁷ F. Mezei, Neutron Spin Echo Study of Spin Glass Dynamics (Invited), *J. Appl. Phys.* **53**, 7654 (1982).
 - ⁸ F. Mezei, The Dynamical Behaviour Associated with the Spin Glass Transition, *J. Magn. Magn. Mater.* **31-34**, 1327 (1983).
 - ⁹ R. H. Heffner and D. E. MacLaughlin, Comparison of Spin-Glass Dynamics Determined by the Muon-Spin-Relaxation and Neutron Spin-Echo Techniques, *Phys. Rev. B* **29**, 6048 (1984).
 - ¹⁰ S. M. Shapiro, H. Maletta, and F. Mezei, Neutron-Spin-Echo Study of the Reentrant Spin Glass $\text{Eu}_x\text{Sr}_{1-x}\text{S}$, *J. Appl. Phys.* **57**, 3485 (1985).
 - ¹¹ C. Pappas, F. Mezei, G. Ehlers, P. Manuel, and I. A. Campbell, Dynamic Scaling in Spin Glasses, *Phys. Rev. B* **68**, 054431 (2003).
 - ¹² J. N. Wagner, W. Häußler, O. Holderer, A. Bauer, S. M. Shapiro, and P. Böni, Influence of Concentration Fluctuations on Relaxation Processes in Spin Glasses, *Quantum Beam Sci.* **2**, 26 (2018).
 - ¹³ R. M. Pickup, R. Cywinski, C. Pappas, B. Farago, and P. Fouquet, Generalized Spin-Glass Relaxation, *Phys. Rev. Lett.* **102**, 097202 (2009).
 - ¹⁴ K. Weron, How to Obtain the Universal Response Law in the Jonscher Screened Hopping Model for Dielectric Relaxation, *J. Phys.: Condens. Matter* **3**, 221 (1991).
 - ¹⁵ C. R. Fincher, S. M. Shapiro, A. H. Palumbo, and R. D. Parks, Spin-Wave Evolution Crossing from the Ferromagnetic to Spin-Glass Regime of $\text{Fe}_x\text{Cr}_{1-x}$, *Phys. Rev. Lett.* **45**, 474 (1980).
 - ¹⁶ S. M. Shapiro, C. R. Fincher, A. C. Palumbo, and R. D. Parks, Anomalous Spin-Wave Behavior in the Magnetic Alloy $\text{Fe}_x\text{Cr}_{1-x}$, *Phys. Rev. B* **24**, 6661 (1981).
 - ¹⁷ K. Motoya, S. M. Shapiro, and Y. Muraoka, Neutron Scattering Studies of the Anomalous Magnetic Alloy $\text{Fe}_{0.7}\text{Al}_{0.3}$, *Phys. Rev. B* **28**, 6183 (1983).
 - ¹⁸ G. Aeppli, S. M. Shapiro, R. J. Birgeneau, and H. S. Chen, Spin Correlations and Reentrant Spin-Glass Behavior in Amorphous Fe-Mn Alloys. II. Dynamics, *Phys. Rev. B* **29**, 2589 (1984).
 - ¹⁹ J. P. Wicksted, S. M. Shapiro, and H. S. Chen, Investigation of the Ferromagnetic-Spin Glass Transition in $\alpha\text{-(Fe}_{77}\text{Cr}_{23})_{75}\text{P}_{16}\text{B}_6\text{Al}_3$, *J. Appl. Phys.* **55**, 1697 (1984).
 - ²⁰ S. Raymond, W. Bao, S. M. Shapiro, and K. Motoya, Spin Dynamics of the Re-Entrant Spin Glass $\text{Fe}_{0.7}\text{Al}_{0.3}$, *Physica B* **241-243**, 597 (1997).
 - ²¹ A. P. Murani and J. L. Tholence, Spin Dynamics of a Binary Alloy (Spin Glass), *Solid State Commun.* **22**, 25 (1977).
 - ²² V. Wagner, J. Hesse, J. Klenke, and C. Pappas, Dynamics of Spin Freezing in the Re-Entrant Spin Glass FeNiMn , *Physica B* **350**, E1051 (2004).
 - ²³ C. Pappas, J. Klenke, J. Hesse, and V. Wagner, Spin freezing in the Re-entrant Spin Glass FeNiMn Close to the Frustration Limit, *Physica B* **397**, 105 (2007).
 - ²⁴ W. Bao, S. Raymond, S. M. Shapiro, K. Motoya, B. Fåk, and R. W. Erwin, Unconventional Ferromagnetic and Spin-Glass States of the Reentrant Spin Glass $\text{Fe}_{0.7}\text{Cr}_{0.3}$, *Phys. Rev. Lett.* **82**, 4711 (1999).
 - ²⁵ E. Fawcett, H. L. Alberts, V. Y. Galkin, D. R. Noakes, and J. V. Yakhmi, Spin-Density-Wave Antiferromagnetism in Chromium Alloys, *Rev. Mod. Phys.* **66**, 25 (1994).
 - ²⁶ J. O. Strom-Olsen, D. F. Wilford, S. K. Burke, and B. D. Rainford, The Coexistence of Spin Density Wave Ordering and Spin Glass Ordering in Chromium Alloys Containing Iron, *J. Phys. F: Met. Phys.* **9**, L95 (1979).
 - ²⁷ G. R. Stewart, Non-Fermi-Liquid Behavior in d - and f -Electron Metals, *Rev. Mod. Phys.* **73**, 797 (2001).
 - ²⁸ H. v. Löhneysen, A. Rosch, M. Vojta, and P. Wölfle, Fermi-Liquid Instabilities at Magnetic Quantum Phase Transitions, *Rev. Mod. Phys.* **79**, 1015 (2007).
 - ²⁹ D. M. Broun, What Lies beneath the Dome? *Nature Phys* **4**, 170 (2008).
 - ³⁰ I. Mirebeau, V. Pierron-Bohnes, C. Decorse, E. Rivière, C.-C. Fu, K. Li, G. Parette, and N. Martin, Magnetic and Atomic Short Range Order in $\text{Fe}_{1-x}\text{Cr}_x$ Alloys, *Phys. Rev. B* **100**, 224406 (2019).
 - ³¹ M. V. Nevitt and A. T. Aldred, Ferromagnetism in V-Fe and Cr-Fe Alloys, *J. Appl. Phys.* **34**, 463 (1963).
 - ³² S. Arajis and G. R. Dunmyre, Electrical Resistivity of Chromium-rich Chromium-iron Alloys between 4° and 320°K , *J. Appl. Phys.* **37**, 1017 (1966).
 - ³³ M. A. Mitchell and J. F. Goff, Electrical Resistivity and the Depression of the Néel Temperature in Cr-Mo and Cr-Fe, *Phys. Rev. B* **5**, 1163 (1972).
 - ³⁴ B. Loegel, Magnetic Transitions in the Chromium-Iron System, *J. Phys. F: Met. Phys.* **5**, 497 (1975).
 - ³⁵ Y. Ishikawa, S. Hoshino, and Y. Endoh, Antiferromagnetism in Dilute Iron Chromium Alloys, *J. Phys. Soc. Jpn.* **22**, 1221 (1967).
 - ³⁶ S. K. Burke and B. D. Rainford, Determination of the Antiferromagnetic Phase Boundary in Cr-Fe Alloys, *J. Phys. F: Met. Phys.* **8**, L239 (1978).
 - ³⁷ S. K. Burke, R. Cywinski, and B. D. Rainford, Superparamagnetism and the Character of Magnetic Order in Binary Cr-Fe Alloys near the Critical Concentration, *J. Appl. Crystallogr.* **11**, 644 (1978).
 - ³⁸ S. K. Burke and B. D. Rainford, The Evolution of Magnetic Order in CrFe Alloys. I. Antiferromagnetic Alloys Close to the Critical Concentration, *J. Phys. F: Met. Phys.* **13**, 441 (1983).
 - ³⁹ S. K. Burke, R. Cywinski, J. R. Davis, and B. D. Rainford, The Evolution of Magnetic Order in CrFe Alloys. II. Onset of Ferromagnetism, *J. Phys. F: Met. Phys.* **13**, 451 (1983).
 - ⁴⁰ S. K. Burke and B. D. Rainford, The Evolution of Magnetic Order in CrFe Alloys. III. Ferromagnetism Close to the Critical Concentration, *J. Phys. F: Met. Phys.* **13**, 471 (1983).
 - ⁴¹ G. Benka, A. Bauer, P. Schmakat, S. Säubert, M. Seifert, P. Jorba, and C. Pfeleiderer, Interplay of Itinerant Magnetism and Spin-Glass Behavior in $\text{Fe}_x\text{Cr}_{1-x}$, *Phys. Rev. Materials* **6**, 044407 (2022).
 - ⁴² I. Mirebeau, S. Itoh, S. Mitsuda, T. Watanabe, Y. Endoh, M. Hennion, and R. Papoulet, Neutron Depolarization in a Reentrant Spin-Glass System: Amorphous Fe-Mn, *Phys. Rev. B* **41**, 11405 (1990).
 - ⁴³ J. A. Mydosh, *Spin Glasses: An Experimental Introduction* (Taylor & Francis, 1993).
 - ⁴⁴ K. Motoya, S. M. Shapiro, and Y. Muraoka, Neutron Scattering Studies of the Anomalous Magnetic Alloy $\text{Fe}_{0.7}\text{Al}_{0.3}$, *Phys. Rev. B* **28**, 6183 (1983).

- ⁴⁵ B. Hennion, M. Hennion, F. Hippert, and A. P. Murani, Observation of Ferromagnetic Spin Waves in a "Reentrant" Ni-Mn Alloy, *Phys. Rev. B* **28**, 5365 (1983).
- ⁴⁶ J. M. D. Coey, *Magnetism and Magnetic Materials* (Cambridge University Press, 2010).
- ⁴⁷ L. C. J. David Musgraves, Juejun Hu, ed., *Springer Handbook of Glass* (Springer, Cham, 2019).
- ⁴⁸ M. F. Collins, V. J. Minkiewicz, R. Nathans, L. Passell, and G. Shirane, Critical and Spin-Wave Scattering of Neutrons from Iron, *Phys. Rev.* **179**, 417 (1969).
- ⁴⁹ T. G. Perring, A. T. Boothroyd, D. M. Paul, A. D. Taylor, R. Osborn, R. J. Newport, J. A. Blackman, and H. A. Mook, High-energy Spin Waves in bcc Iron, *J. Appl. Phys.* **69**, 6219 (1991).
- ⁵⁰ J. Kindervater, S. Säubert, and P. Böni, Dipolar Effects on the Critical Fluctuations in Fe: Investigation by the Neutron Spin-Echo Technique MIEZE, *Phys. Rev. B* **95**, 014429 (2017).
- ⁵¹ S. Säubert, J. Kindervater, F. Haslbeck, C. Franz, M. Skoulatos, and P. Böni, Dipolar Interactions in Fe: A Study with the Neutron Larmor Precession Technique MIEZE in a Longitudinal Field Configuration, *Phys. Rev. B* **99**, 184423 (2019).
- ⁵² E. Fawcett, Spin-Density-Wave Antiferromagnetism in Chromium, *Rev. Mod. Phys.* **60**, 209 (1988).
- ⁵³ B. E. A. Fisher, A Theory of Spin Waves in Chromium, *J. Phys. F* **2**, 806 (1972).
- ⁵⁴ J. Als-Nielsen and O. W. Dietrich, Spin Waves and the Order-Disorder Transition in Chromium, *Phys. Rev. Lett.* **22**, 290 (1969).
- ⁵⁵ S. Lequien, B. Hennion, and S. M. Shapiro, Reinvestigation of the Reentrant Spin-Glass Phase of $\text{Fe}_{26}\text{Cr}_{74}$ by High-resolution Inelastic Neutron Scattering, *Phys. Rev. B* **38**, 2669 (1988).
- ⁵⁶ F. Mezei, G. Drabkin, and A. Ioffe, Polarimetric Neutron Spin Echo, *Physica B* **297**, 9 (2001).
- ⁵⁷ B. Farago and F. Mezei, Study of Magnon Dynamics in Fe near T_C by Modified Neutron Spin Echo Techniques, *Physica B+C* **136**, 100 (1986).
- ⁵⁸ W. Besenböck, R. Gähler, P. Hank, R. Kahn, M. Köppe, C.-H. D. Novion, W. Petry, and J. Wuttke, First Scattering Experiment on MIEZE: A Fourier Transform Time-of-Flight Spectrometer Using Resonance Coils, *J. Neutron Res.* **7**, 65 (1998).
- ⁵⁹ R. Gähler, R. Golub, and T. Keller, Neutron Resonance Spin Echo - a New Tool for High Resolution Spectroscopy, *Physica B* **180-181**, 899 (1992).
- ⁶⁰ C. Franz and T. Schröder, RESEDA: Resonance Spin Echo Spectrometer, *J. Large-Scale Res. Facil.* **1**, 14 (2015).
- ⁶¹ C. Franz, O. Soltwedel, C. Fuchs, S. Säubert, F. Haslbeck, A. Wendl, J. K. Jochum, P. Böni, and C. Pfeleiderer, The Longitudinal Neutron Resonant Spin Echo Spectrometer RESEDA, *Nucl. Instrum. Methods Phys. Res.* **939**, 22 (2019).
- ⁶² M. Krautloher, J. Kindervater, T. Keller, and W. Häußler, Neutron Resonance Spin Echo with Longitudinal DC Fields, *Rev. Sci. Instrum.* **87**, 125110 (2016).
- ⁶³ W. Häußler, P. Böni, M. Klein, C. J. Schmidt, U. Schmidt, F. Groitl, and J. Kindervater, Detection of High Frequency Intensity Oscillations at RESEDA Using the CASCADE Detector, *Rev. Sci. Instrum.* **82**, 045101 (2011).
- ⁶⁴ I. Mirebeau and N. Martin, Revisiting Neutron Studies of Reentrant Spin Glasses: the Role of Small-angle Scattering, *J. Appl. Crystallogr.* **55**, 1173 (2022).
- ⁶⁵ S. Mercone, V. Hardy, C. Martin, C. Simon, D. Saurel, and A. Brület, Field Dependence of the Electronic Phase Separation in $\text{Pr}_{0.67}\text{Ca}_{0.33}\text{MnO}_3$ by Small-Angle Magnetic Neutron Scattering, *Phys. Rev. B* **68**, 094422 (2003).
- ⁶⁶ M. Viret, F. Ott, J. P. Renard, H. Glättli, L. Pinsard-Gaudart, and A. Revcolevschi, Magnetic Filaments in Resistive Manganites, *Phys. Rev. Lett.* **93**, 217402 (2004).
- ⁶⁷ R. Pickup, R. Cywinski, and C. Pappas, A Novel Approach to Modelling Non-exponential Spin Glass Relaxation, *Physica B* **397**, 99 (2007).
- ⁶⁸ I. A. Campbell, J. M. Flesselles, R. Jullien, and R. Botet, Random Walks on a Hypercube and Spin Glass Relaxation, *J. Phys. C: Solid State Phys.* **20**, L47 (1987).
- ⁶⁹ I. A. Campbell, J. M. Flesselles, R. Jullien, and R. Botet, Nonexponential Relaxation in Spin Glasses and Glassy Systems, *Phys. Rev. B* **37**, 3825 (1988).
- ⁷⁰ K. Tajima, P. Böni, G. Shirane, Y. Ishikawa, and M. Kohgi, Paramagnetic Spin Fluctuations in an $\text{Fe}_{65}\text{Ni}_{35}$ Invar Alloy, *Phys. Rev. B* **35**, 274 (1987).
- ⁷¹ C. Lartigue, F. Mezei, C. Pappas, and M. Alba, Unusual Critical Dynamics in AuFe Re-Entrant Ferromagnets, *Physica B* **180-181**, 359 (1992).
- ⁷² C. Pappas, C. Lartigue, M. Alba, and F. Mezei, Critical Dynamics of AuFe Reentrant Ferromagnets Close to the Percolation Threshold, *Physica B* **165-166**, 191 (1990).